Detection of small breast tumors using tumor penetrating-polymersomes engineered to target p32 protein

Lorena Simón-Gracia[1], Pablo Scodeller[1], Desirè Di Silvio[2], Sergio Salazar[3], Vanessa Gómez Vallejo[4], Xabier Ríos[4], Eneko San Sebastián[4], Meina Suck[5], Federica De Lorenzi[5], Larissa Yokota Rizzo[5], Saskia von Stillfried[5], Kalle Kilk[6], Twan Lammers[5], Sergio E Moya[2]*, Tambet Teesalu[1,7,8]*

[1]Laboratory of Cancer Biology, Institute of Biomedicine and Translational Medicine, University of Tartu, Ravila 14b, 50411 Tartu, Estonia. [2]Soft Matter Laboratoy, CIC Biomagune, Miramon Pasealekua, 182, 20009 Donostia, Spain. [3]Animal Unit, CIC Biomagune, Miramon Pasealekua, 182, 20009 Donostia, Spain. [4]Laboratory of Radiochemistry, CIC Biomagune, Miramon Pasealekua, 182, 20009 Donostia, Spain. Department of Nanomedicine and Theranostics [5]Institute for Experimental Molecular Imaging, RWTH Aachen University Clinic, Pauwelsstrasse 30, 52074 Aachen, Germany. [6]Laboratory of Biochemistry, Institute of Biomedicine and Translational Medicine, University of Tartu, Ravila 14, Tartu, 50411, Estonia. [7] Cancer Research Center, Sanford Burnham Prebys Medical Discovery Institute, 10901 N. Torrey Pines Road, La Jolla, 92097 California, USA. [8]Center for Nanomedicine and Department of Cell, Molecular and Developmental Biology, University of California, Santa Barbara Santa Barbara, 93106 California, USA.

RUNNING TITLE: p32-targeted breast tumor PET contrast agent

Key words: PET, homing peptide, C-end Rule, neuropilin-1, p32, triple negative breast cancer

Abstract

Triple negative breast cancer (TNBC) is the deadliest form of breast cancer and its successful treatment critically depends on early diagnosis and therapy. The hyaluronic acid-binding p32 protein is overexpressed in TNBC, specifically in macrophages in hypoxic areas of the tumor. Here we used polyethylene glycol-polycaprolactone (PEG-PCL) polymersomes that were affinity targeted with the p32-binding tumor penetrating peptide LinTT1 (AKRGARSTA) for delivery of imaging and therapeutic payloads to TNBC lesions. A tyrosine residue was added to the peptide to allow for ^{124}I labeling and PET imaging. Systemic LinTT1-targeted polymersomes accumulated in early tumor lesions more than twice as efficient as untargeted polymersomes with up to 20% ID/cc at 24 h after administration. The PET-imaging was very sensitive, allowing detection of tumors as small as ~20mm^3. Confocal imaging of tumor tissue sections revealed a high degree of vascular exit and stromal penetration of LinTT1-targeted polymersomes and co-localization with tumor-associated macrophages. Our studies show that systemic LinTT1-targeted polymersomes can be potentially used for precision-guided tumor imaging and treatment of TNBC.

Introduction

Triple negative breast cancer (TNBC) accounts for a 15% of all breast cancer cases and shows the least favorable prognosis among the breast cancer subtypes. On average, patients with TNBC have cancer recurrence within 3 years after initial diagnosis and a life expectancy of approximately 5 years[1]. TNBC tumors are locally invasive and highly metastatic and must be detected and treated early to prevent dissemination.

Nanoformulations offer unique advantages for drug delivery. Nanoparticles can be designed to encapsulate hydrophobic molecules that would otherwise be insoluble, and payloads that have short circulation half-life and/or need to be protected from enzymes in the bloodstream, such as esterases or nucleases[2]. Cancer diagnosis and treatment can be combined into one modality by dual-use “theranostic” nanocarriers engineered to simultaneously deliver therapeutic and imaging cargoes[3][4]. Imaging payloads, such as fluorescent, MRI, and radio tags can be loaded in the nanosystems or coated on their surface. Nanosized polymeric vesicles (polymersomes) self-assembled from biocompatible copolymers are particularly appealing because of their versatility and unique properties. The high molecular weight of block copolymers results in the formation of highly entangled membranes displaying an increased resilience with elastomer-like mechanical properties. This confers the polymersomes a high

flexibility[5][6] and higher ability for tissue penetration than other vesicles self-assembled from low MW entities[7]. Polymersomes can be loaded with hydrophilic effector molecules, e.g. low molecular weight drugs[8][9], proteins[10], nucleic acids[11], and imaging agents[12][13], in their aqueous lumen and with hydrophobic cargoes within the polymer membrane[8][14].

The surface of nanoparticles can also be modified to improve their in vivo behavior: to modulate circulation half-life, to reduce non-specific interactions and delivery to non-target sites, and to achieve selective accumulation in target tissue(s). Affinity ligands, such as homing peptides[15][16] and antibodies[17] can be coated on the nanoparticles for specific tissue and cell recognition. Tumor penetrating peptides[18] can be used to concentrate cytotoxic molecules and drug-loaded nanoparticles in tumors and potentiate their antitumor activity[14][19]. The AKRGARSTA peptide, referred to as “LinTT1” (linear TT1), is a 9 amino acid tumor penetrating peptide that binds to p32 protein, which is overexpressed on the surface of malignant and stromal cells in tumors[20]. LinTT1 gets processed by tumor-derived proteases, such as urokinase type plasminogen activator (uPA), to C-terminally expose the C-end rule motif of the peptide (i.e. AKRGAR), which is capable of interacting with the cell- and tissue-penetration receptor neuropilin-1 (NRP1)[20][21]. The primary receptor of LinTT1, the p32 protein, is expressed on the membrane of tumor cells and also on macrophage/myeloid cells in hypoxic areas of tumors[22]. Recently, LinTT1-functionalization was found to significantly improve the therapeutic index of iron oxide nanoworms loaded with proapoptotic effector peptide in a TNBC model[23]. In that study, the biodistribution of fluorescently labeled Lin-TT1 nanoparticles was evaluated by optical imaging of tissue sections. However, fluorescence imaging-based in vivo biodistribution studies remain challenging due to issues related to the low depth of light penetration, tissue autofluorescence, and the semi-quantitative nature of optical imaging[24].

Positron Emission Tomography (PET) and Single Photon Emission Computed Tomography (SPECT) are clinically used for imaging of radioactive contrast agents with beta and gamma emission, respectively. In contrast to magnetic resonance imaging (MRI), computed tomography (CT), and imaging using optical contrast agents, PET and SPECT are not subject to endogenous tissue background.

Encouraged by the anticancer activity of LinTT1-targeted therapeutic nanoparticles on orthotopic breast tumors in mice [23], we decided to evaluate polymersomes guided with the LinTT1 peptide as a potential theranostic nanocarrier to the TNBC lesions. We performed PET imaging of LinTT1 targeted PEG-PCL polymersomes in a mouse model of orthotopic TNBC,

from early time points to up to 48 h post-injection. Intravenously-administered p32-targeted ^{124}I labeled polymersomes showed good tumor selectivity and, importantly, allowed detection of small (~20mm^3) tumors. Our results suggest potential applications of LinTT1 engineered polymersomes for theranostics of TNBC.

Materials and Methods

Materials

PEG_{5000}-PCL_{10000} (PEG-PCL) and Maleimide-PEG_{5000}-PCL_{10000} (Mal-PEG-PCL) copolymers were purchased from Advanced Polymer Materials Inc. (Montreal, Canada). Cys-Tyr-TT1 and Cys-Tyr peptides were purchased from KareBay Biochem, Inc. (USA), and Cys-fluorescein (FAM)-TT1 and Cys-FAM peptides were purchased from TAG Copenhagen (Denmark). Sodium iodine-124 was purchased from Perkin Elmer (Amsterdam). Thin liquid chromatography sheets were purchased from Agilent Technologies (USA). The ATTO550-amine dye was purchased from Atto-Tech GmbH (Germany).

Synthesis and characterization of peptide-PEG-PCL vesicles

PEG-PCL (8 mg, 0.53 µmol) and Mal-PEG-PCL (2 mg, 0.13 µmol) copolymers were dissolved in 1 mL of acetone previously purged with nitrogen. The solvent was evaporated and the polymer film was hydrated with 1 mL of saline phosphate buffer 10 mM pH 7.4, previously purged with nitrogen. The suspension was sonicated for 5 minutes and the peptide (Cys-Tyr-LinTT1, Cys-Tyr, Cys-FAM-LinTT1peptide, or Cys-FAM, 0.4 mg, 2 eq), dissolved in 0.2 mL PBS previously purged was added to the suspension. The suspension was sonicated for 30 min, mixed at R.T. for 2 h and kept overnight at 4°C. The vesicles were purified using centrifugal filters of 100 kDa MWCO (Amicon Ultra, Merck Millipore. Ltd. Ireland) and the final suspension was concentrated to 100 mg of copolymer/mL.

For the polymersomes labeled with ATTO550, the dye was first conjugated to the polymer. Mal-PEG-PCL (10 mg, 0.65 µmol) was dissolved in 0.3 mL of DMF previously purged with nitrogen and ATTO550-NH_2 (0.77 mg, 2 eq) dissolved in 0.1 mL of previously purged DMF was added to the solution. Triethylene amine (1 µL) was added to the solution as a catalyzer. The solution was reacted at room temperature overnight, dialyzed against water using dialysis membrane of 3.5 KDa MWCO (Sigma-Aldrich), and freeze-dried. ATTO550-PEG-PCL (1mg, 0.06 µmol), PEG-PCL (8 mg, 0.53 µmol) and Mal-PEG-PCL (2 mg, 0.13 µmol) were dissolved in 0.5 mL of

acetone. The solvent was then evaporated to form the polymer film. The polymersomes were assembled and the Cys-LinTT1 peptide conjugation was performed as described above.

Dynamic Light Scattering (DLS) and Z-potential measurements (Zetasizer Nano ZS, Malvern Instruments, USA) were used to assess the average size, polydispersity, and surface charge of polymersome preparations. The size was measure at a concentration of 1mg polymer/mL in PBS (10 mM of phosphate and 137 mM of NaCl). The z-potential was measured at 0.2 mg of polymer/mL in NaCl 10 mM). Transmission electron microscopy (TEM) was used to assess the size and morphology of assembled vesicles. Briefly, polymersomes were deposited from a water solution onto copper grids at 1 mg/mL, stained with 0.75% phosphotungstic acid (pH 7), air-dried, and imaged by TEM (Tecnai 10, Philips, Netherlands). The number of polymersomes in the suspension was measured using the ZetaWiew instrument (Particle Metrix GmbH, Germany).

Iodination of PEG-PCL vesicles

Two milligrams of Iodogen (cat no. T0656, Sigma-Aldrich) were dissolved in 10 mL of CH_2Cl_2 and 20 µL of this solution was transferred to a tube and the solvent was evaporated. LinTT1-Tyr-polymersomes or Tyr-polymersomes (1mg) were mixed with $Na^{124}I$ (18.5 MBq) and 10 µL of buffer phosphate 0.5 M in a tube containing iodogen. After 30 minutes 250 µL of phosphate buffer, 1M NaCl, pH 7.4 was added to the reaction and the solution was transferred to a tube containing 50 µL of $Na_2S_2O_3$ 0.1 M. The radiolabeling yield was measured by thin layer chromatography using glass microfiber chromatography paper impregnated with silica gel (Agilent Technologies, USA) and ethanol:water 85:15 as liquid phase. The radioactivity of the peaks was measured with a TLC reader (γ-MiniGITA, Raytest, Germany). The polymersomes were purified using centrifugal filters of 100 kDa molecular weight cut off (Amicon Ultra, Merck Millipore. Ltd. Ireland) and resuspended in 0.1 mL of PBS. The removal of the free ^{124}I was confirmed by radio-TCL and the final radioactivity was measured with a dose calibrator (Capintec CRC-25R, USA)

In vitro binding of polymersomes to recombinant p32 protein

Recombinant hexahistidine–tagged p32 was bacterially expressed and purified as described in [20]. For protein binding assays, Ni-NTA magnetic agarose beads (Qiagen, Germany) in binding buffer (50 mM Tris pH 7.4, 150 mM NaCl, 5 mM imidazole) were coated with p32 protein at 15 µg of protein/10 µL beads. Radiolabelled polymersomes were incubated with the p32-coated

beads in binding buffer containing 1% BSA at RT for 1 h. The magnetic beads were washed with binding buffer and resuspended in a final volume of 1 mL of binding buffer. The radioactivity of each sample was quantified by automatic gamma counter (2470 Wizard 2, Perkin Elmer).

Uptake of polymersomes in cultured cells

4T1 cells (ATCC, CRL-2539) were cultured in RPMI medium 1640 + GlutaMAX with 25 mM HEPES (Gibco, Life Technologies, USA) containing 100 IU/mL of penicillin and streptomycin, and 10% of heat-inactivated fetal bovine serum (GE Healthcare, UK). 4T1 cells ($5x10^5$) were seeded on glass coverslips in a 24-well plate and the next day incubated with ATTO550-labelled polymersomes (0.5 mg polymer/mL) at 37 °C for 1 h. Cells were washed with PBS, fixed with 4% paraformaldehyde, permeabilized with 0.5% saponin, and blocked for 1 h with 1% bovine serum albumin, 1% goat serum, 0.3M of glycine, and 0.05% of Tween-20 in PBS. Cells were then stained for p32 protein using anti-p32 rabbit polyclonal (Millipore, Germany) and Alexa Fluor 488 goat anti-rabbit IgG (Abcam, UK) as a secondary antibody, and counterstained with 1 µg/mL of DAPI. Cells were examined under the confocal laser scanning microscope (LSM 510 Meta,Zeiss, Germany) equipped with a 63x oil objective lens (1.4 NA). Images were acquired sequentially to avoid cross-talk using excitation wavelengths 405, 488 and 561 nm. Transmission images were collected and overlaid by Zeiss Zen software.

In vivo PET/CT imaging

For tumor induction, 1 million 4T1 cells in 50 µL of PBS were orthotopically implanted in the mammary gland of Balb/c mice (Charles River Laboratories, Spain). After 3 days, when the tumor volume had reached ~18 mm^3, the mice were injected in tail vein with 3.7-7.4 MBq of radiolabelled polymersomes (1 mg polymer, 100 µL, N = 5 mice) and subjected to PET/CT scans. During the scan acquisitions the mice were kept anesthetized with 1.5−2% isofluorane blended with O_2. The PET/CT scans were performed at 10 min, 2, 6, 12, 24, and 48 h using the Argus PET/CT scanner (Sedecal, Molecular Imaging, Spain). First, PET scans were acquired using the following acquisition protocol: whole body emission scan, 2 beds, 10 min of total acquisition time for the scans at 10 min, 2, 6, 12, and 24 h post-injection and 20 minutes for the 48 h time point. The acquisition method was static, using 400-700 KeV energetic window, FBP reconstruction algorithm, with correction for scatter coincidences. For the CT scans the used current was 140 µA, 40 kV of voltage, rotation of 360 degrees, 4 shoots, 1 bed, acquisition time of 6 minutes, and a reconstruction binning of 2. After 48 h of radiolabeled polymersome injection the mice were sacrificed and the tumor, blood, and organs were excised and further used for

biodistribution studies. The PET/CT images were processed with the Medical Image Data Examiner AMIDE software. The CT and PET images were overlaid, the tumor volume was manually extracted from the CT scans and the same ROI was applied in the PET images, averaged, and expressed as percentage of injected dose per cubic centimeter of tissue (ID/cc). For the rendered 3D PET/CT images, PMOD image analysis software (PMOD Technologies Ltd, Zürich, Switzerland) was used. A 3D Gauss Filter of 1.5x1.5x1.5 mm was applied to the PET image in order to increase the signal to noise ratio for 3D visualization.

Biodistribution studies

For biodistribution studies the tumor, blood, and organs were weighed and the radioactivity was measured using the automatic gamma counter. A standard curved was generated using ^{124}I to determine the relationship between cpm and Bq. The biodistribution was expressed as percentage of injected dose per gram of tissue (ID/g). To determine the elimination rate of polymersomes, the radioactive signal in the whole mouse body was measured from the PET images at 10 min, 2, 6, 12, 24, and 48 h post-injection and normalized by the signal at 10 minutes post-injection. The elimination rate was expressed as signal in mouse x 100 divided by the signal at time zero.

Tissue immunofluorescence and confocal microscopy

Balb/c mice were orthotopically injected with 1 million of 4T1 cells in the mammary gland and after 3 days FAM-LinTT1-PS (1 mg of polymer, 100 µL) was intravenously injected. After 24 h, the animals were sacrificed and the tumor and organs were excised, fixed in 4% of paraformaldehyde, cryoprotected with 15% and 30% sucrose, frozen down with liquid nitrogen, and cryosectioned at 10µm. Tissue sections were permeabilized using PBS 10 mM containing 0.2% Triton-X for 10 min, and blocked in PBS 10 mM containing 0.05% Tween-20, 5% FBS, 5% BSA, and 5% goat serum (GE Healthcare, UK) for 1 h. The sections were immunostained with anti-fluorescein rabbit IgG fraction (cat. no. A889, Thermo Fisher Scientific, MA, USA), rat anti-mouse CD31, biotin rat anti-mouse CD11b, (BD Biosciences, CA, USA), rat anti-mouse CD68, rat anti-mouse CD206 (Bio-Rad, USA), and anti-p32 rabbit polyclonal antibody (Millipore, Germany) as primary antibodies. As secondary antibodies, Alexa 488-conjugated goat anti-rabbit IgG and Alexa 647-conjugated goat anti-rat IgG (Invitrogen, Thermo Fisher Scientific, MA, USA) were used. The sections were counterstained with DAPI and examined by fluorescence confocal microscopy using Olympus FV1200MPE instrument. The images were processed and

analyzed using the FV10-ASW 4.2 Viewer image software (Olympus, Germany) and the Image J software.

Ex vivo binding of polymersomes to human breast tumor

Surgical samples of breast cancer patients were collected under protocols approved by the Ethics Committee of the University of Tartu, Estonia (permit #243/T27). Fresh samples were frozen in liquid nitrogen, cryosectioned at 10 µm, and fixed with 4% paraformaldehyde. Sections were permeabilized using PBS containing 0.2% Triton-X for 10 min, and blocked in PBS 10 mM containing 5% FBS, 5% BSA, and 5% goat serum (GE Healthcare, UK) for 1 h. The samples were incubated overnight at 4° C with LinTT1-FAM-PS or FAM-PS (1 mg of polymer/mL) in PBS 10 mM containing 1% FBS, 1% BSA, and 1% goat serum. After washes with PBS 10 mM containing 0.05% Tween-20, the sections were fixed with 4% paraformaldehyde and immunostained with anti-fluorescein rabbit IgG fraction and Alexa 488-conjugated goat anti-rabbit IgG. The sections were counterstained with DAPI and examined by fluorescence confocal microscopy using Olympus FV1200MPE instrument. Images were processed and analyzed using the FV10-ASW 4.2 Viewer image software (Olympus, Germany) and Image J software.

Staining and quantification of CD68 in human tissue of breast tumor, lymph node, and healthy tissue.

Surgical samples of TNBC with lymph node metastasis (tumor MET; n=10), TNBC without lymph node metastasis (tumor nonMET; n=10) as well as their corresponding metastasized lymph nodes (LN MET; n=10) and non-metastasized lymph nodes (LN nonMET; n=10) and healthy breast tissue (healthy; n =10), were fixed for 12-24 hours in 4% neutral buffered formalin. In two cases with neoadjuvant chemotherapy and in two cases where only very small residual tumor was found in the surgical specimen, specimens from corresponding diagnostic biopsies were selected for immunohistochemistry. Samples were dehydrated, embedded in paraffin, sectioned at 4 µm, and mounted on coated microscope slides (Dako, Denmark). After deparaffinization and rehydration of the sections, target retrieval was performed in citrate buffer at pH 6.1 in a pre-treatment module (PT-Link, Dako, Denmark). Using an autostainer (Thermo Fisher Scientific) slides were incubated with endogenous peroxidase blocking solution for 5 minutes, followed by primary mouse anti-human CD68 antibody (1:100, Dako, M0876) for 30 minutes. Next, slides were incubated with goat secondary antibody molecules against mouse (and rabbit) immunoglobulins conjugated to a peroxidase-labeled polymer chain (Dako, Denmark) for 20 minutes. The antigen-antibody-polymer complex was visualized with DAB +

Chromogen (Dako, Denmark) for 10 minutes. The counterstaining was performed with Hematoxylin (Dako, Denmark) for 5 minutes. Finally, slides were covered with coverslipping film (Sakura, 6132 Prisma®). All stainings were performed on archived FFPE human samples and approved by the local ethics committee (EK 039/17).

Immunostaining of cell surface p32

4T1 and MCF10CA1a cells (10^4) were seeded on glass coverslips in a 24 well-plates and incubated at 37°C overnight. The cells were blocked in PBS containing 0.05% Tween-20, 5% FBS, 5% BSA, and 5% goat serum (GE Healthcare, UK) for 1 h. Cells were immunostained with rabbit anti-p32 (10 µg/mL, in house). As a secondary antibody, Alexa 647-conjugated goat anti-rat IgG (Invitrogen, Thermo Fisher Scientific, MA, USA) was used. Cells were counterstained with DAPI, transferred to glass slides, and examined by fluorescence confocal microscopy using the Zeiss LSM710 instrument.

Assessment of in vitro cell surface p32 expression by flow cytometry

4T1 and MCF10CA1a cells were detached from the culture plate with enzyme-free cell dissociation buffer (Gibco, Life Technologies, UK). The cells (10^5 cells) were incubated with 10µg/mL the in-house generated rabbit polyclonal p32 antibody in blocking buffer containing 1% of BSA, 1% of FBS, and 1% of goat serum in PBS at room temperature for 1 h. The cells were washed, and incubated with Alexa 647-conjugated goat anti-rat IgG in blocking buffer at room temperature for 30 min. After washes, the cell surface p32 expression was analyzed by flow cytometry (Accuri, BD Biosciences, CA, USA).

Statistical analysis

All the statistical analysis was performed with the Statistica 8 software, using the one-way ANOVA, Fisher LSD test.

Results

Preparation, functionalization and radiolabeling of polymersomes

Polymersomes were prepared by the film hydration method and functionalized with the LinTT1-Tyr or LinTT1-FAM peptide through a thioether bond between the maleimide group of the copolymer and the thiol group of the cysteine of the peptide. The number of polymersomes was

determined by the ZetaView instrument and the loading of FAM-labelled peptide was quantified by fluorimetry. The peptide functionalization resulted in ~3.7x10^4 peptides/polymersome particle (density ~1.2 peptides/nm^2). For radiolabeling, the polymersomes were functionalized with the LinTT1-Tyr-Cys peptide or control Tyr-Cys dipeptide. The tyrosine residue was incorporated for radioiodination. The hydrodynamic diameter of LinTT1-Tyr-polymersomes (LinTT1-Tyr-PS, Tyr-polymersomes (Tyr-PS), polymersomes labeled with ATTO550 (LinTT1-ATTO550-PS and ATTO550-PS), and polymersomes labeled with FAM (LinTT1-FAM-PS and FAM-PS) measured by DLS, was ~130 nm for all the polymersome samples (Figure 1B). The Z-potential was slightly negative but very close to 0 for the different polymersome preparations (Figure 1B and S1).

For PET imaging, the LinTT1-Tyr-PS and Tyr-PS were radiolabeled with ^{124}I. Before purification, the efficiency of polymersome radiolabeling was determined by TLC (Figure S2). The yield of radiolabeling after purification, measured with activimeter, was 48±9% for LinTT1-Tyr-^{124}I-PS and 43±2% for Tyr-^{124}I-PS. The low radiolabeling of PEG-PCL polymersomes without peptide indicated that ^{124}I present in LinTT1-Tyr-^{124}I-PS and Tyr-^{124}I-PS preparations was predominantly due to the covalent binding of ^{124}I to the tyrosine residue of the peptides (Figure S2). TLC analysis after purification demonstrated that 99% of the ^{124}I was bound to polymersomes (Fig. 1C).

LinTT1-targeted polymersomes bind to recombinant p32 and to cultured breast tumor cells.

To evaluate the effect of LinTT1 functionalization on the tropism of polymersomes in vitro, we first tested the binding of LinTT1-Tyr-^{124}I-polymersomes to recombinant p32 protein, the primary receptor of LinTT1. P32-coated magnetic beads were incubated with the polymersomes, and polymersome binding was quantified by gamma counter. Compared to non-targeted polymersomes, LinTT1-Tyr-^{124}I-polymersomes showed ~10-fold increased binding to the p32 beads (Figure 2A). This binding was specific, as the LinTT1-Tyr-^{124}I-polymersomes did not bind to NRP-1 (Figure 2A). The LinTT1 peptide does not bind to NRP-1 unless proteolytically processed by uPA[21]. These data show that the LinTT1 peptide attached to the polymersomes remains available for p32 binding to modulate polymersome tropism.

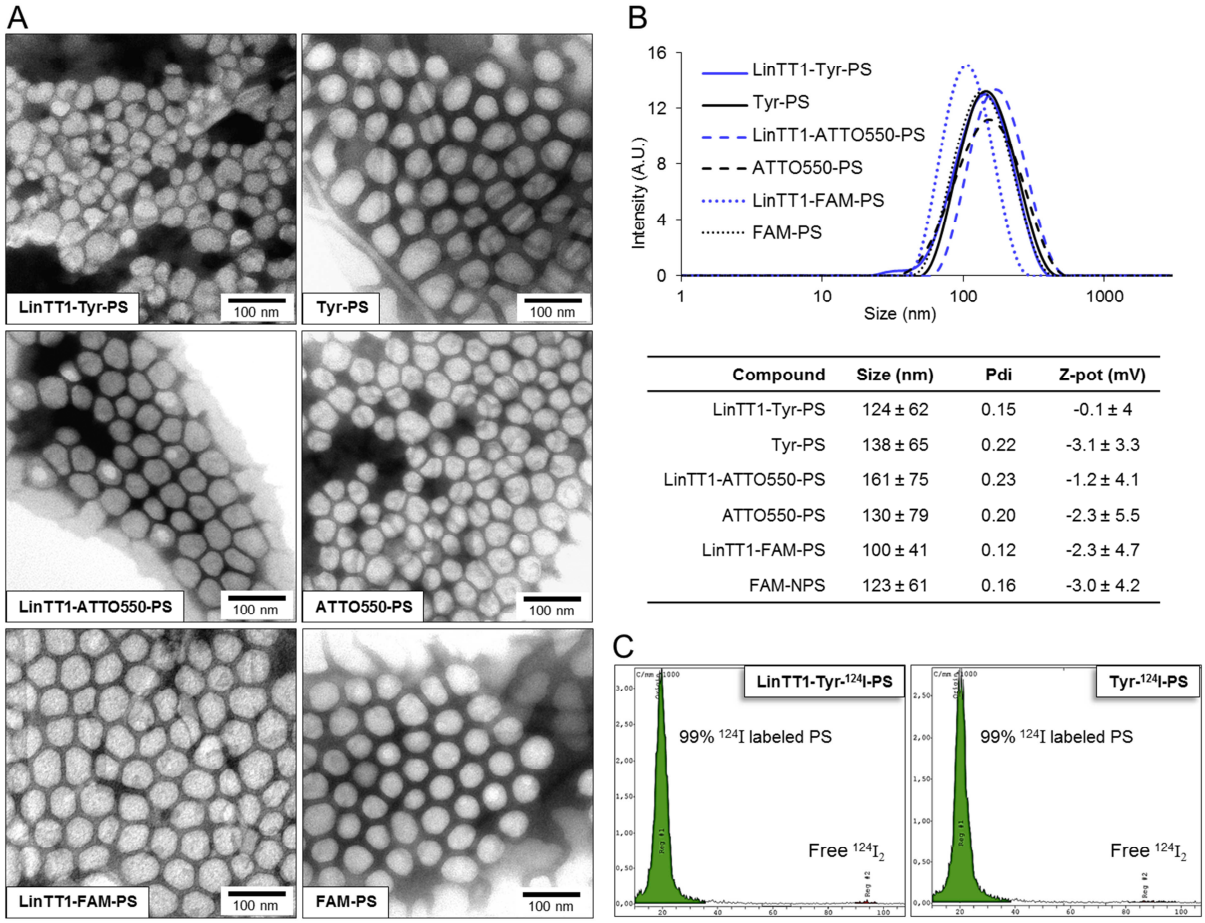

Compound	Size (nm)	Pdi	Z-pot (mV)
LinTT1-Tyr-PS	124 ± 62	0.15	-0.1 ± 4
Tyr-PS	138 ± 65	0.22	-3.1 ± 3.3
LinTT1-ATTO550-PS	161 ± 75	0.23	-1.2 ± 4.1
ATTO550-PS	130 ± 79	0.20	-2.3 ± 5.5
LinTT1-FAM-PS	100 ± 41	0.12	-2.3 ± 4.7
FAM-NPS	123 ± 61	0.16	-3.0 ± 4.2

Figure 1. Characterization of the polymersomes. A) TEM of the LinTT1-targeted and non-targeted radiolabeled polymersomes (LinTT1-Tyr-124I-PS and Tyr-124I-PS) and fluorescently labeled polymersomes (LinTT1-ATTO550-PS, ATTO550-PS, LinTT1-FAM-PS, and FAM-PS). B) DLS and summary of the physical properties of the polymersome preparations (3 independent measurements). C) TLC of radiolabeled polymersomes after the purification showing the percentage of ^{124}I-labeled PS and the peak of free ^{124}I.

Various human and mouse tumor cell lines express p32 on the cell surface [22]. We studied the the presence of cell surface p32 in 4T1 and MCF-10CA1a TNBC cells by flow cytometry and confocal microscopy, and confirmed its surface expression on both cell lines (Figure S3).To study the uptake of polymersomes in 4T1 cells, we incubated the cultured cells for 1h with LinTT1-targeted or control polymersomes labeled with ATTO550 (LinTT1-ATTO550-PS and ATTO550-PS) (Figure 2B). The LinTT1-functionalization increased polymersome uptake in 4T1 cells and the signal from LinTT1-ATTO550-PS partially colocalized with p32 (Figure 2B). These

experiments demonstrate that LinTT1 functionalization results in p32-enhanced uptake of polymersomes in cultured 4T1 cells.

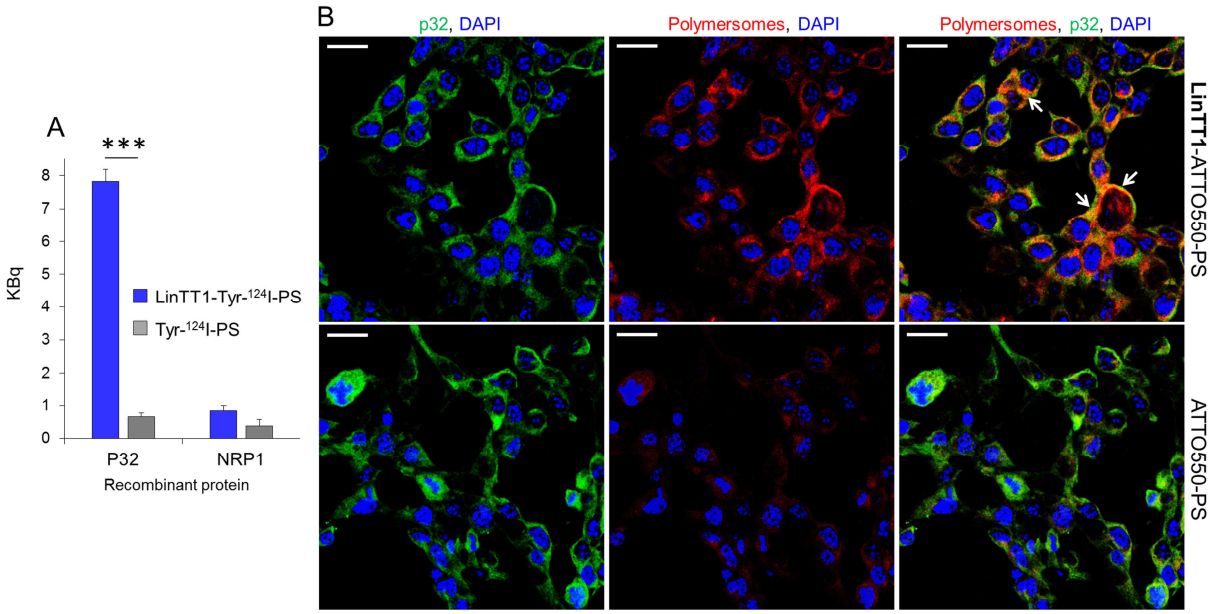

Figure 2. Binding of LinTT1-PS to recombinant p32 protein and to cultured 4T1 breast tumor cells. A) Binding of the LinTT1-Tyr-^{124}I-PS and Tyr-^{124}I-PS to p32 and NRP-1-coated magnetic beads. The binding to the proteins after 1 h of polymersome incubation is expressed in KBq. N=3. Error bar = +SEM. P value < 0.001. B) Fluorescence confocal microscopy images of 4T1 cells incubated with LinTT1-ATTO550-PS or non-targeted ATTO550-PS for 1 h. The polymersomes were labeled with ATTO550 (red) and cells were immunostained for p32 protein (green). The nuclei were counterstained with DAPI (blue). Scale bar: 20 µm. White arrows point to the areas of colocalization of LinTT1-ATTO550-PS with p32.

Systemic LinTT1 targeted radiolabeled polymersomes home to breast tumors.

We used PET imaging to study in vivo biodistribution and tumor accumulation of systemic LinTT1-targeted polymersomes. Radiolabeled LinTT1-Tyr-^{124}I-PS and Tyr-^{124}I-PS were i.v. injected into mice bearing orthotopic 4T1 breast tumors and PET-CT scans were acquired at 10 min, 2, 6, 12, 24, and 48 h post-injection. To test whether detection of incipient breast tumors could be improved by targeting p32, the polymersomes were administered when breast tumor had reached ~20 mm^3 (Figure S3).

LinTT1 functionalization increased tumor homing of polymersomes at both early and late time points (Figure 3C), with the area under the curve (AUC) in tumor being ~60% higher (Figure 3D). We saw tumor accumulation of LinTT1-Tyr-^{124}I-PS already at 2 h post injection, whereas

the tumor PET signal for non-targeted Tyr-^{124}I-PS was only detectable at later time points (Figure 3A). The highest tumor accumulation of LinTT1-Tyr-^{124}I-PS was seen at 24 h after the injection, and it was 67% higher than for the untargeted polymersomes. At 48 h both targeted and untargeted polymersomes showed accumulation in the tumor (Fig 3A,B,E). At 48 h tumor accumulation of LinTT1-Tyr-^{124}I-PS was lower than at 24 h, however, it was significantly higher than Tyr-^{124}I-PS (12±0.9 and 9±0.4 ID/cc, respectively) (Figure 3C). In contrast, at 48 h, the signal in the kidney and thyroid gland in mice injected with targeted and untargeted polymersomes was not significantly different (Figure 3E, Figure S4).

The scans acquired at 6 h showed uptake of both targeted and non-targeted polymersomes in the liver (Figure 3A), in line with known role of this organs of the reticuloendothelial system (RES) in the clearance of the circulating nanoparticles.

At 48 h after the injection, the tumors and organs were excised and ^{124}I in tissue extracts was quantified with gamma counter. The highest percentage of ID/g of both targeted and non-targeted polymersomes after 48 h was observed in spleen and tumor (Figure 4A). Accumulation of both LinTT1 and untargeted polymersomes in spleen is consistent with the polymersome clearance by the RES. After 48 h, untargeted polymersomes showed accumulation in tumors (15±0.6% ID/g) and the functionalization with LinTT1 increased tumor accumulation of polymersomes by >70%, to 26±3% ID/g. Moreover, the percentage of ID/g of LinTT1-Tyr-^{124}I-PS in tumor was 2.5 times higher than in liver (Figure 4A). Quantification of radioactivity revealed more than 2-fold higher accumulation of LinTT1-Tyr-^{124}I-PS than Tyr-^{124}I-PS in the lymph nodes of breast tumor mice (Figure 4A).

The elimination rate of ^{124}I was studied by quantification of the PET imaging data. At 24 h, ~50% of the injected Tyr-^{124}I-PS and 67% of LinTT1-Tyr-^{124}I-PS remained in the body. After 48 h, 32% of Tyr-^{124}I-PS and 45% for LinTT1-Tyr-^{124}I-PS remained in the body (Figure 4B). We have shown in a recent publication that an insignificant portion of the peptide is released from PEG-PCL polymersomes incubated with the serum of the 4T1 tumor bearing mice for 6 h. We suggest that the high excretion at short time points observed is due to the renal clearance of the ^{124}I released from the peptide-conjugated polymersomes. It is important to note that the signal in thyroid gland (Figure S4) - which accumulates free iodine - is similar for both targeted and untargeted polymersomes, suggesting similar leaching of Iodine.

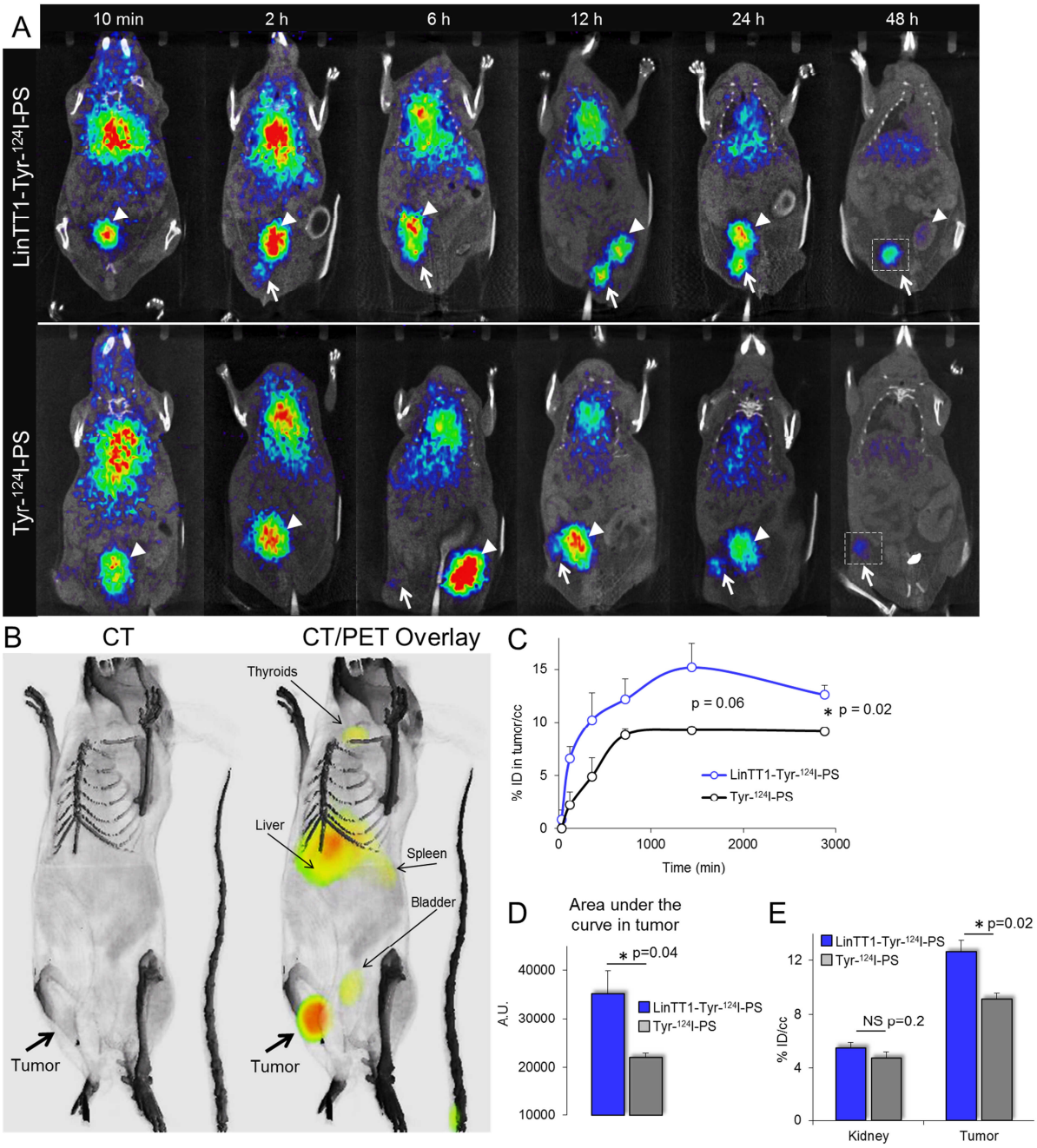

Figure 3. Radiolabeled LinTT1-PS home to 4T1 breast tumors. A) PET-CT imaging of 4T1 tumor mice injected with LinTT1-Tyr-^{124}I-PS or non-targeted Tyr-^{124}I-PS. White arrows point to the tumor. White arrowheads point to the bladder. B) 3D reconstruction of CT and PET/CT overlay images of mouse at 48 h after LinTT1-Tyr-^{124}I-PS i.v. injection. C) Accumulation of radiolabeled polymersomes in the tumor. The % of ID/cc tumor was plotted against the time post-injection. The signal was quantified from the PET images. D) AUC of LinTT1-Tyr-^{124}I-PS and non-targeted Tyr-^{124}I-PS calculated from the graphic C. E) % ID/cc in kidney and tumor after 48 h of polymersome injection. The signal was quantified from the PET images. N=5 mice. Error bar = +SEM.

LinTT1-polymersomes target both the tumor cells and tumor macrophages

We next studied the tissue biodistribution of i.v. administered FAM-labeled polymersomes in 4T1 orthotopic tumor mice at the cellular level. The polymersomes were injected in 4T1 tumor mice, allowed to circulate for 24 h, and the sections of tumors and control organs were analyzed by confocal immunoanalysis.

We first studied the biodistribution of p32 immunoreactivity in tissues. In a previous report, p32 was found to be upregulated in MDA-MB-435 breast tumors compared to the control organs[25][22]. P32 immunostaining of sections of tumors and control organs from 4T1 mice demonstrated elevated expression of p32 in tumor tissue (Figure S5).

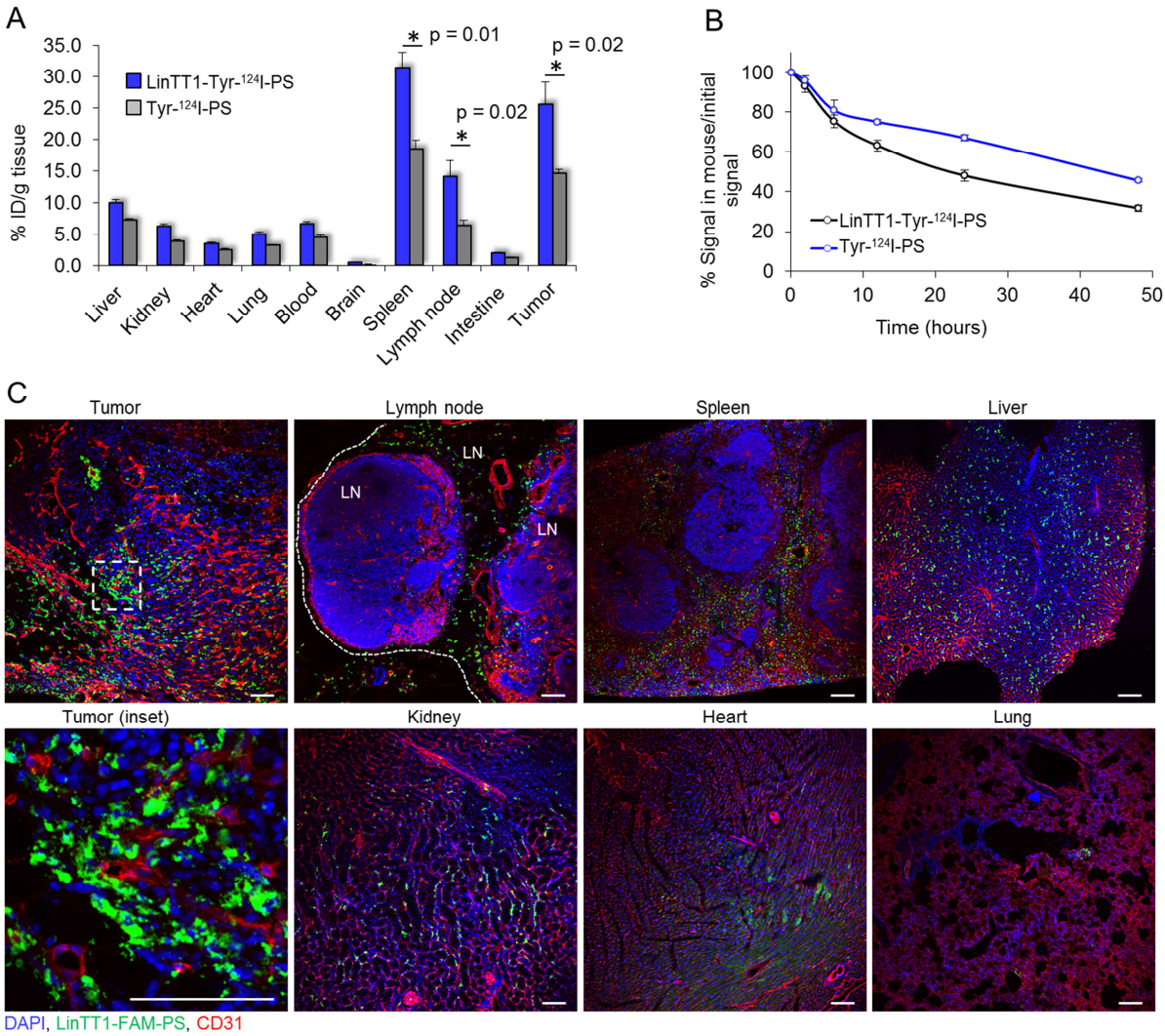

Figure 4. Biodistribution of radioactive and fluorescent polymersomes in 4T1 tumor mice. A) Biodistribution of i.v.-injected ^{124}I labeled polymersomes in tumors and organs at 48 h after injection. Tumors, control organs, and blood were collected at 48 h post injection of radiolabeled polymersomes and the radioactivity was measured by gamma counter. N=6. Error bar = +SEM. B) Elimination rate of ^{124}I quantified from the PET data. The radioactive signal of the whole mouse was determined at different time points. N=5 mice. Error bar = +SEM. C) Confocal fluorescence imaging of sections of 4T1 tumors and control organs from mice injected i.v. with FAM-polymersomes. Tissues were collected at 24 h post injection of polymersomes into 4T1 bearing mice and sectioned and immunostained for FAM and CD31. Green: LinTT1-FAM-PS; red: CD31; blue: DAPI nuclear staining. LN= lymph node.

In agreement with the tissue extract-based radiography data, FAM-LinTT1-polymersomes accumulated in tumor and spleen (Fig. 3A). It was recently published that LinTT1 functionalization of nanoparticles enhances their penetration into the tumor tissue[23][15]. Here we show that at 24 h, the LinTT1-FAM-PS in tumors did not colocalize with CD31-positive blood vessels, confirming that polymersomes had extravasated and penetrated into tumor stroma (Figure 4C, tumor inset). It was recently shown that p32 is expressed by CD11b positive macrophages[25] and that LinTT1-conjugated nanoparticles colocalized with C68-positive macrophages in the breast[23], gastric, and colon tumors[15]. To study the macrophage uptake of LinTT1-PS, sections of tumors and organs were immunostained with antibodies against CD68, CD11b, and CD206 markers. CD68 and CD11b are pan-macrophage markers that label normal macrophages (including macrophages in spleen, lung, and in Kupffer cells in liver[26]), and tumor-associated macrophages[27]. CD206 is a marker of pro-tumoral M2 macrophages[28] known promote tumor progression[29]. We found that LinTT1-FAM-PS colocalized with CD68 (>50% of colocalization), and showed partial colocalization with CD11b and CD206 (9% and 21% of colocalization, respectively) in tumor, confirming targeting of the tumor-associated macrophages (Figure 5A and 5B). CD68-positive macrophages found in lymph nodes, spleen, and liver also showed some degree of colocalization with LinTT1-FAM-PS (Figure S6A and S6B).

LinTT1-polymersomes bind to human breast tumor sections

To investigate the translational relevance of LinTT1-targeted polymersomes we evaluated the binding of LinTT1-FAM-PS to sections of human breast tumor. Clinical samples from breast tumor were sectioned and overlayed overnight with LinTT1-FAM-PS or non-targeted FAM-PS and analyzed by immunostaining. LinTT1 functionalization increased polymersome binding to breast tumor sections ~10 times (Figure 6A and B).

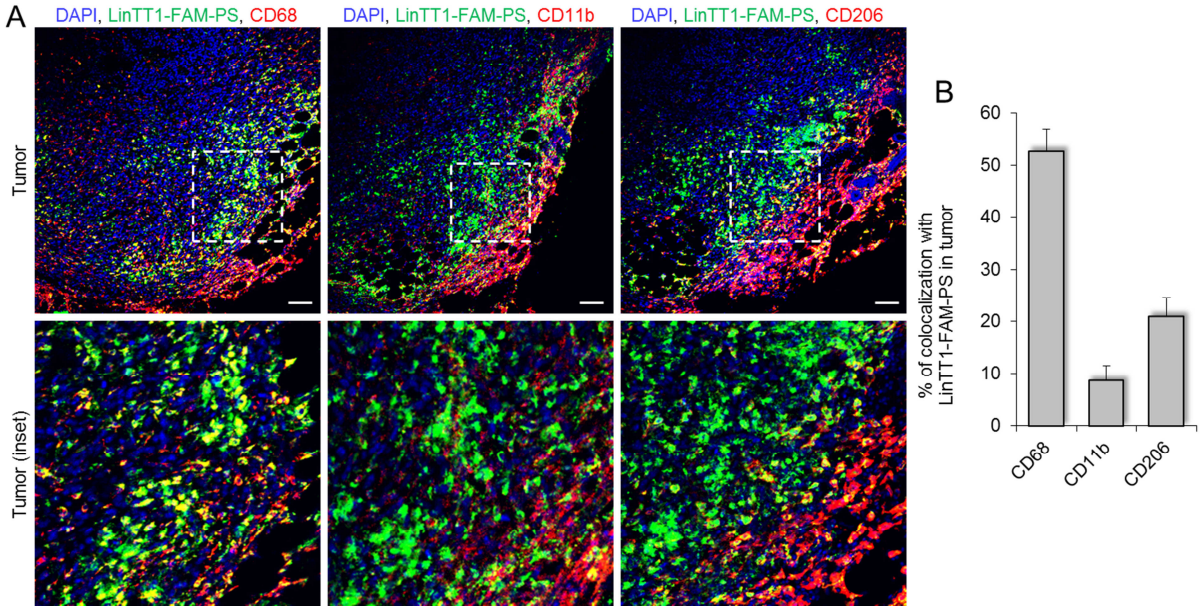

Figure 5. Colocalization of LinTT1-polymersomes with macrophage markers in tumor tissue. 4T1 tumors were collected at 24 h after LinTT1-FAM-PS i.v. injection into 4T1 bearing mice, sectioned and immunostained. A) Confocal images of tumor sections immunostained for FAM, CD68, CD11b, and CD206, and counterstained with DAPI. B) Quantification of the colocalization of LinTT1-FAM-PS and macrophage markers in tumor using FLUOVIEW Viewer software. Green: LinTT1-FAM-PS; red: CD68, CD11b, CD206; blue: DAPI counterstaining. LN= lymph node. Error bar = +SEM.

We also analysed the distribution of p32 and CD68 immunoreactivity in primary triple negative breast tumors and lymph nodes from clinical samples from patients with or without metastasis, and control human tissues. P32 was expressed in all the groups, but it was significantly overexpressed in primary tumors, both metastatic and non-metastatic, and in metastaic lymph nodes, compared with healthy tissue (Figure S7). Compared to healthy tissue, increased number of CD68-positive cells was found in breast tumors and in lymph nodes, both from patients with and without metastases (Figure S8).

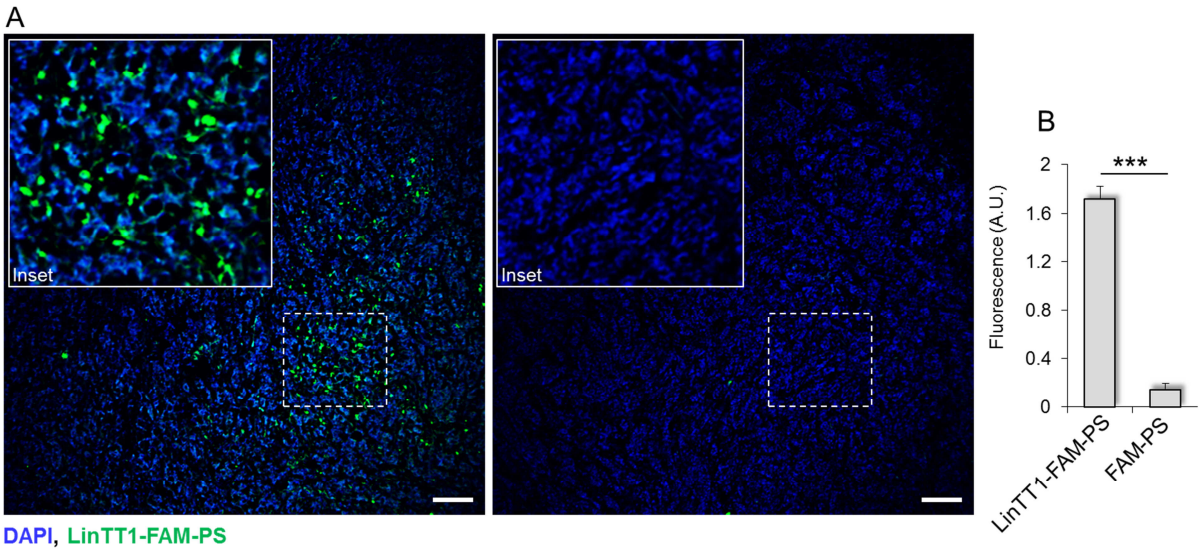

Figure 6: Ex vivo binding of LinTT1-polymersomes to human breast tumors. A) Confocal imaging of clinical breast tumor sections incubated overnight with LinTT1-FAM-PS or FAM-PS and immunostained for FAM (green) and counterstained for DAPI (blue). B) Quantification of the FAM fluorescence in tissue sections with Image J software. P value<0.001.

Discussion

In the current study we evaluated the Lin TT1-guided biocompatible PEG-PCL polymersomes as PET contrast agent for TNBC detection. Our findings indicate that LinTT1-polymersomes can be used for sensitive and specific detection of triple negative breast tumors. This, along with recently published reports on LinTT1-mediated targeting of therapeutic nanocarriers[15][23], suggests potential theranostic applications for the LinTT1-targeted nanocarriers.

Nanoparticles have been affinity targeted to tumors for PET imaging: in a recent PET study, clinical application of RGD-targeted PET-active nanoparticles for melanoma imaging was reported[36]. The current study documents high tumor accumulation of LinTT1-polymersomes (>20% ID/cc) that translates into ability to detect very small malignant lesions, hardly visible by CT. This sets our system apart from other molecular and nanoparticle PET contrast agents with reported tumor accumulation range between 5-10 % ID/g [37][38][39]. Remarkable tumor selectivity and tumor binding capacity observed for the LinTT1-polymersomes is likely to be due to a combination of the tumor homing properties of LinTT1 peptide with the favorable properties of the PEG-PCL polymersome nanoplatform. LinTT1 belongs to a family of tumor homing

peptides that, unlike conventional vascular homing peptides, are not limited to vascular docking sites but have access to extended tumor extravascular space[31]. Another potentially contributing aspect, not addressed in the current study, is the ability of LinTT1 to increase tumor penetration of co-administered compounds and nanocarriers. LinTT1-iron oxide nanoparticles were recently found to increase tumor penetration of co-administered 70kDa dextrane[15]. Homing of LinTT1-nanocarriers may thus not be limited by the number of systemically accessible peptide receptors and allow more nanocarriers to enter the tumor tissue for improved sensitivity of detection. Tumor accumulation of LinTT1-polymersomes may also be enhanced by physicochemical features PEG-PCL polymersomes used in the current study. On one hand, the flexibility of polymersomes[7] may contribute to tissue penetrative targeting with TPPs. In addition, polymersomes are known to possess an intrinsic tumor tropism. For example recently we have demonstrated that pH-sensitive POEGMA-PDPA polymersomes efficiently delivered payloads to the tumor tissue in the absence of active targeting[8]; this accumulation was further boosted by targeting with iRGD peptide [14]. Likewise, the systemic radiolabeled non-targeted polymersomes in the current study showed high accumulation in 4T1 breast tumors; this accumulation was potentiated by functionalization of polymersomes with the LinTT1 peptide by about 70%.

LinTT1 homing is likely due to a combination of both tumor cell and macrophage targeting. In the 4T1 breast tumor mice, the highest ID/g of LinTT1-polymersomes was seen in the tumor, spleen, and lymph nodes. All these tissues contain abundant macrophages, a cell population known to upregulate, upon activation, the expression of cell surface p32 Tumor-associated macrophages (TAM), an important diagnostic and therapeutic target, play major roles in progression of solid tumors. LinTT1-polymersomes may be capable of targeting tumor cells and TAMs in TNBC patients, as the peptide is not species specific, and since TAMs are abundant in clinical lymph node and breast tumor samples. We show here that primary breast tumors and lymph nodes from clinical samples from patients with or without metastasis overexpress p32 protein and that the number of CD68+ macrophages is increased compared with healthy tissues. In the context of drug delivery, TAMs can act as slow-release reservoir of drugs encapsulated in polymeric particles[35]. Our finding of the binding of LinTT1-polymersomes to sections of clinical samples also supports potential translatability of the system into clinical applications. Clinical breast tumors are heterogeneous and the cell surface p32 expression and the sensitivity to p32-targeting-based treatment is likely to differ between the patients. PET imaging with LinTT1-polymersomes can be potentially used as a companion diagnostic test for

selection of patient cohort most likely to respond to p32-targeted therapies. Furthemore, accumulation of LinTT1-polymersomes in sentinel lymph nodes containing 4T1 tumor cells migrating out from the primary tumor and activated macrophages, suggests potential applications for LinTT1-polymersomes for improved detection of early metastatic dissemination of breast cancer than is possible with currently approved compounds, such as Lymphoseek[40].

The potential applications of our system extend beyond breast cancer detection and therapeutic targeting. Systemically accessible p32 is overexpressed across solid tumors, including, gastric, colon, and overian caricinoma[15], glioma (Säälik et al. unpublished), and atherosclerosis[41]. Systematic evaluation of the relevance of the linTT1-polymersomes for detection and/or therapy of these conditions will be a subject of follow-up studies.

Funding

This work was supported by the European Union through the H2020 PEOPLE RISE project HYMADE (645686) and the European Regional Development Fund (Project No. 2014-2020.4.01.15-0012),by EMBO Installation grant #2344 (to T. Teesalu), European Research Council starting grant GLIOMADDS from European Regional Development Fund (to T. Teesalu), Wellcome Trust International Fellowship WT095077MA (to T. Teesalu).

Acknowledgements

L. Simón-Gracia acknowledges Rein Laiverik (Department of Anatomy, University of Tartu) and Angel (CIC Biomagune) for the assistance with the TEM equipment in this work. D. Di Silvio, and S. Moya acknowledge the ERA-NET SIINN FATENANO for support.

[1] R. Dent, M. Trudeau, K.I. Pritchard, W.M. Hanna, H.K. Kahn, C.A. Sawka, L.A. Lickley, E. Rawlinson, P. Sun, S.A. Narod, Triple-Negative Breast Cancer: Clinical Features and Patterns of Recurrence, Clin. Cancer Res. 13 (2007). http://clincancerres.aacrjournals.org/content/13/15/4429.figures-only#sec-3 (accessed August 16, 2017).

[2] A.P. Mann, P. Scodeller, S. Hussain, J. Joo, E. Kwon, B. Gary, A peptide for targeted, systemic delivery of imaging and therapeutic compounds into acute brain injuries, Nat. Commun. 7 (2016) 1–11. doi:10.1038/ncomms11980.

[3] T. Lammers, S. Aime, W.E. Hennink, G. Storm, F. Kiessling, Theranostic Nanomedicine, Acc. Chem. Res. 44 (2011) 1029–1038. doi:10.1021/ar200019c.

[4] S. Kunjachan, J. Ehling, G. Storm, F. Kiessling, T. Lammers, Noninvasive Imaging of Nanomedicines and Nanotheranostics: Principles, Progress, and Prospects, Chem. Rev. 115 (2015) 10907–10937. doi:10.1021/cr500314d.

[5] B.M. Discher, Y.Y. Won, D.S. Ege, J.C. Lee, F.S. Bates, D.E. Discher, D.A. Hammer, Polymersomes: tough vesicles made from diblock copolymers., Science. 284 (1999) 1143–6. http://www.ncbi.nlm.nih.gov/pubmed/10325219 (accessed April 24, 2016).

[6] H. Bermudez, A.K. Brannan, D.A. Hammer, F.S. Bates, D.E. Discher, Molecular Weight Dependence of Polymersome Membrane Structure, Elasticity, and Stability, Macromolecules. 35 (2002) 8203–8208. doi:10.1021/ma020669l.

[7] C. Pegoraro, D. Cecchin, J. Madsen, N. Warren, S.P. Armes, S. MacNeil, A. Lewis, G. Battaglia, Translocation of flexible polymersomes across pores at the nanoscale., Biomater. Sci. 2 (2014) 680–92. doi:10.1039/c3bm60294j.

[8] L. Simon-Gracia, H. Hunt, P.D. Scodeller, J. Gaitzsch, G.B. Braun, A.-M.A. Willmore, E. Ruoslahti, G. Battaglia, T. Teesalu, Paclitaxel-Loaded Polymersomes for Enhanced Intraperitoneal Chemotherapy., Mol. Cancer Ther. (2016). doi:10.1158/1535-7163.MCT-15-0713-T.

[9] C. Pegoraro, D. Cecchin, L.S. Gracia, N. Warren, J. Madsen, S.P. Armes, A. Lewis, S. MacNeil, G. Battaglia, Enhanced drug delivery to melanoma cells using PMPC-PDPA polymersomes, Cancer Lett. 334 (2013) 328–337. doi:10.1016/j.canlet.2013.02.007.

[10] L. Wang, L. Chierico, D. Little, N. Patikarnmonthon, Z. Yang, M. Azzouz, J. Madsen, S.P. Armes, G. Battaglia, Encapsulation of biomacromolecules within polymersomes by electroporation., Angew. Chem. Int. Ed. Engl. 51 (2012) 11122–5. doi:10.1002/anie.201204169.

[11] H. Lomas, A.P.R. Johnston, G.K. Such, Z. Zhu, K. Liang, M.P. Van Koeverden, S. Alongkornchotikul, F. Caruso, Polymersome-Loaded Capsules for Controlled Release of DNA, Small. 7 (2011) 2109–2119. doi:10.1002/smll.201100744.

[12] I. Canton, G. Battaglia, Polymersomes-mediated delivery of fluorescent probes for targeted and long-term imaging in live cell microscopy, Methods Mol. Biol. 991 (2013) 343–351. doi:10.1007/978-1-62703-336-7_31.

[13] L. Chierico, A.S. Joseph, A.L. Lewis, G. Battaglia, Live cell imaging of membrane/cytoskeleton interactions and membrane topology., Sci. Rep. 4 (2014) 6056. doi:10.1038/srep06056.

[14] L. Simón-Gracia, H. Hunt, P. Scodeller, J. Gaitzsch, V.R. Kotamraju, K.N. Sugahara, O. Tammik, E. Ruoslahti, G. Battaglia, T. Teesalu, iRGD peptide conjugation potentiates intraperitoneal tumor delivery of paclitaxel with polymersomes, Biomaterials. 104 (2016) 247–257. doi:10.1016/j.biomaterials.2016.07.023.

[15] H. Hunt, L. Simón-Gracia, A. Tobi, V.R. Kotamraju, S. Sharma, M. Nigul, K.N. Sugahara, E. Ruoslahti, T. Teesalu, Targeting of p32 in peritoneal carcinomatosis with intraperitoneal linTT1 peptide-guided pro-apoptotic nanoparticles, J. Control. Release. 260 (2017) 142–153. doi:10.1016/j.jconrel.2017.06.005.

[16] X. Tian, S. Nyberg, P. S Sharp, J. Madsen, N. Daneshpour, S.P. Armes, J. Berwick, M. Azzouz, P. Shaw, N.J. Abbott, G. Battaglia, LRP-1-mediated intracellular antibody delivery to the Central Nervous System., Sci. Rep. 5 (2015) 11990. doi:10.1038/srep11990.

[17] T.T. Smith, S.B. Stephan, H.F. Moffett, L.E. McKnight, W. Ji, D. Reiman, E. Bonagofski, M.E. Wohlfahrt, S.P.S. Pillai, M.T. Stephan, In situ programming of leukaemia-specific T cells using synthetic DNA nanocarriers, Nat. Nanotechnol. (2017). doi:10.1038/nnano.2017.57.

[18] T. Teesalu, K.N. Sugahara, E. Ruoslahti, Tumor-penetrating peptides., Front. Oncol. 3 (2013) 216. doi:10.3389/fonc.2013.00216.

[19] K.N. Sugahara, T. Teesalu, P.P. Karmali, V.R. Kotamraju, L. Agemy, O.M. Girard, D. Hanahan, R.F. Mattrey, E. Ruoslahti, Tissue-Penetrating Delivery of Compounds and Nanoparticles into Tumors, Cancer Cell. 16 (2009) 510–520. doi:10.1016/j.ccr.2009.10.013.

[20] L. Paasonen, S. Sharma, G.B. Braun, V.R. Kotamraju, T.D.Y. Chung, Z.-G. She, K.N. Sugahara, M. Yliperttula, B. Wu, M. Pellecchia, E. Ruoslahti, T. Teesalu, New p32/gC1qR Ligands for Targeted Tumor Drug Delivery, ChemBioChem. 17 (2016) 570–575. doi:10.1002/cbic.201500564.

[21] G.B. Braun, K.N. Sugahara, O.M. Yu, V.R. Kotamraju, T. Mölder, A.M. Lowy, E. Ruoslahti, T. Teesalu, Urokinase-controlled tumor penetrating peptide., J. Control. Release. 232 (2016) 188–95. doi:10.1016/j.jconrel.2016.04.027.

[22] V. Fogal, L. Zhang, S. Krajewski, E. Ruoslahti, Mitochondrial/Cell-Surface Protein p32/gC1qR as a Molecular Target in Tumor Cells and Tumor Stroma, Cancer Res. 68 (2008).

[23] S. Sharma, V.R. Kotamraju, T. Mölder, A. Tobi, T. Teesalu, E. Ruoslahti, Tumor-Penetrating Nanosystem Strongly Suppresses Breast Tumor Growth, Nano Lett. (2017)

acs.nanolett.6b03815. doi:10.1021/acs.nanolett.6b03815.

[24] E.T. Ahrens, J.W.M. Bulte, Tracking immune cells in vivo using magnetic resonance imaging, Nat. Rev. Immunol. 13 (2013) 755–763. doi:10.1038/nri3531.

[25] V. Fogal, A.D. Richardson, P.P. Karmali, I.E. Scheffler, J.W. Smith, E. Ruoslahti, Mitochondrial p32 protein is a critical regulator of tumor metabolism via maintenance of oxidative phosphorylation., Mol. Cell. Biol. 30 (2010) 1303–18. doi:10.1128/MCB.01101-09.

[26] Table 1 : Protective and pathogenic functions of macrophage subsets : Nature Reviews Immunology, (n.d.). http://www.nature.com/nri/journal/v11/n11/fig_tab/nri3073_T1.html (accessed April 11, 2017).

[27] D.G. DeNardo, J.B. Barreto, P. Andreu, L. Vasquez, D. Tawfik, N. Kolhatkar, L.M. Coussens, CD4(+) T cells regulate pulmonary metastasis of mammary carcinomas by enhancing protumor properties of macrophages., Cancer Cell. 16 (2009) 91–102. doi:10.1016/j.ccr.2009.06.018.

[28] L. Martinez-Pomares, The mannose receptor, J. Leukoc. Biol. 92 (2012) 1177–1186. doi:10.1189/jlb.0512231.

[29] C.E. Lewis, A.S. Harney, J.W. Pollard, The Multifaceted Role of Perivascular Macrophages in Tumors, Cancer Cell. 30 (2016) 18–25. doi:10.1016/j.ccell.2016.05.017.

[30] G.L. Cascini, A. Niccoli Asabella, A. Notaristefano, A. Restuccia, C. Ferrari, D. Rubini, C. Altini, G. Rubini, 124 Iodine: a longer-life positron emitter isotope-new opportunities in molecular imaging., Biomed Res. Int. 2014 (2014) 672094. doi:10.1155/2014/672094.

[31] E. Ruoslahti, Tumor penetrating peptides for improved drug delivery, Adv. Drug Deliv. Rev. 110-111 (2017) 3–12. doi:10.1016/j.addr.2016.03.008.

[32] E.I. Peerschke, K.B. Reid, B. Ghebrehiwet, Identification of a novel 33-kDa C1q-binding site on human blood platelets., J. Immunol. 152 (1994) 5896–901. http://www.ncbi.nlm.nih.gov/pubmed/8207215 (accessed July 7, 2017).

[33] W.X. Guo, B. Ghebrehiwet, B. Weksler, K. Schweitzer, E.I. Peerschke, Up-regulation of endothelial cell binding proteins/receptors for complement component C1q by inflammatory cytokines., J. Lab. Clin. Med. 133 (1999) 541–50. http://www.ncbi.nlm.nih.gov/pubmed/10360628 (accessed July 7, 2017).

[34] E.I.B. Peerschke, B. Ghebrehiwet, cC1qR/CR and gC1qR/p33: Observations in cancer, Mol. Immunol. 61 (2014) 100–109. doi:10.1016/j.molimm.2014.06.011.

[35] M.A. Miller, Y.-R. Zheng, S. Gadde, C. Pfirschke, H. Zope, C. Engblom, R.H. Kohler, Y. Iwamoto, K.S. Yang, B. Askevold, N. Kolishetti, M. Pittet, S.J. Lippard, O.C. Farokhzad,

R. Weissleder, Tumour-associated macrophages act as a slow-release reservoir of nano-therapeutic Pt(IV) pro-drug, Nat. Commun. 6 (2015) 8692. doi:10.1038/ncomms9692.

[36] E. Phillips, O. Penate-Medina, P.B. Zanzonico, R.D. Carvajal, P. Mohan, Y. Ye, J. Humm, M. Gönen, H. Kalaigian, H. Schöder, H.W. Strauss, S.M. Larson, U. Wiesner, M.S. Bradbury, Clinical translation of an ultrasmall inorganic optical-PET imaging nanoparticle probe., Sci. Transl. Med. 6 (2014) 260ra149. doi:10.1126/scitranslmed.3009524.

[37] A.B. Benito, M.K. Aiertza, M. Marradi, L. Gil-Iceta, T. Shekhter Zahavi, B. Szczupak, M. Jiménez-González, T. Reese, E. Scanziani, L. Passoni, M. Matteoli, M. De Maglie, A. Orenstein, M. Oron-Herman, G. Kostenich, L. Buzhansky, E. Gazit, H.-J. Grande, V. Gómez-Vallejo, J. Llop, I. Loinaz, Functional Single-Chain Polymer Nanoparticles: Targeting and Imaging Pancreatic Tumors *in Vivo*, Biomacromolecules. 17 (2016) 3213–3221. doi:10.1021/acs.biomac.6b00941.

[38] H. Lee, B. Hoang, H. Fonge, R.M. Reilly, C. Allen, In vivo distribution of polymeric nanoparticles at the whole-body, tumor, and cellular levels, Pharm. Res. 27 (2010) 2343–2355. doi:10.1007/s11095-010-0068-z.

[39] C. Pérez-Medina, D. Abdel-Atti, J. Tang, Y. Zhao, Z.A. Fayad, J.S. Lewis, W.J. Mulder, T. Reiner, Nanoreporter PET predicts the efficacy of anti-cancer nanotherapy, Nat. Commun. 7 (2016) 11838. doi:10.1038/ncomms11838.

[40] A.M. Wallace, C.K. Hoh, K.K. Limmer, D.D. Darrah, G. Schulteis, D.R. Vera, Sentinel lymph node accumulation of Lymphoseek and Tc-99m-sulfur colloid using a "2-day" protocol., Nucl. Med. Biol. 36 (2009) 687–92. doi:10.1016/j.nucmedbio.2009.04.007.

[41] J. Hamzah, V.R. Kotamraju, J.W. Seo, L. Agemy, V. Fogal, L.M. Mahakian, D. Peters, L. Roth, M.K.J. Gagnon, K.W. Ferrara, E. Ruoslahti, Specific penetration and accumulation of a homing peptide within atherosclerotic plaques of apolipoprotein E-deficient mice., Proc. Natl. Acad. Sci. U. S. A. 108 (2011) 7154–9. doi:10.1073/pnas.1104540108.